Natural Resources Canada | Ressources naturelles Canada

GEOLOGICAL SURVEY OF CANADA
OPEN FILE 8028

Poroelastic Modeling of Hydraulic Fracturing Induced Earthquake Stress Field

S. Larochelle, Y. Liu, and H. Kao

2016

Canada

GEOLOGICAL SURVEY OF CANADA
OPEN FILE 8028

Poroelastic Modeling of Hydraulic Fracturing Induced Earthquake Stress Field

S. Larochelle[1], Y. Liu[2], and H. Kao[3]

[1] McGill University, Department of Civil Engineering and Applied Mechanics, Montreal, Quebec
[2] McGill University, Department of Earth and Planetary Sciences, Montreal, Quebec
[3] Geological Survey of Canada, Pacific Division, Sidney, British Columbia

2016

doi:10.4095/297811

This publication is available for free download through GEOSCAN (http://geoscan.nrcan.gc.ca/).

Recommended citation
Larochelle, S., Liu, Y., and Kao, H., 2016. Poroelastic modeling of hydraulic fracturing induced earthquake stress field; Geological Survey of Canada, Open File 8028, 27 p. doi:10.4095/297811

Publications in this series have not been edited; they are released as submitted by the author.

1. Introduction

That earthquakes can be induced by anthropogenic activities has been known for decades. Since 1908, numerous seismic events with a very wide magnitude range (from M<0 to M~7) have been reported as unintended consequences of mining activities, reservoir impoundment as well as fluid and gas injections (McGarr et al*.,* 2002). Raleigh et al. (1976) proved that earthquake generation could be controlled by varying the pore pressure through fluid injections at the Rangely Oil Field in Colorado. In recent years, there has been renewed interest in the subject due to the abnormally high levels of seismicity (mostly with M<5) observed in Central and Eastern United States. The increase of seismicity is concurrent with the surge in shale gas extraction which started in 2009 (Rubinstein and Mahani, 2015). In the United States, the additional seismicity correlates particularly well with the deep injections of wastewater associated with hydrocarbon production. In Canada, however, induced seismicity seems to correlate better with the process of hydraulic fracturing itself (Rubinstein and Mahani, 2015; Atkinson et al., 2016).

Although much remains to be understood about induced earthquakes, the general mechanism by which fluid injection can lead to earthquake generation is thought to be related to the injection of large volume at high pressure that disturbs the ambient pore pressure field. As described by the Mohr-Coulomb theory, increasing pore pressure reduces the shear strength of the crust material (Coulomb, 1976). If shear strength drops to the existing stress level, the rock fails and releases seismic energy in the process (Raleigh et al., 1976). When the pore pressure perturbation is hydraulically linked to a fault structure, seismic fault slip may result (Frohlich*,* 2012).

To fully understand the mechanisms involved in injection-induced earthquakes, poroelastic effects as established by Biot (1956) must be considered. A purely diffusive model would ignore the hydro-mechanical relationship that exists between the porous crust material and the pore fluid. When a porous medium is subjected to a mechanical compressive load, pore space is reduced and pore pressure increases. This increase in pore pressure in turn imposes an extra load on the porous medium which further deforms as a result (Detournay and Cheng, 1993). Poroelastic effects are expected to be significant in the particular application of injection-induced earthquakes as the change in stress state due to injection should lead to further changes in pore pressure.

In this study, poroelasticity is implemented in a numerical model of the problem at stake by using the finite-difference software FLAC3D (ITASCA, 2011) supported by the Geological Survey of Canada (GSC) Induced Seismicity Research Project. Given a fixed injection source near a pre-existing fault, this preliminary model simulates slip as well as stresses and pore pressure evolution in the vicinity of the fault. The model is informed by hydraulic fracturing induced seismic events of the Crooked Lake Sequences in Western Canada (Schultz et al*.,* 2015). The present report is part of a larger research initiative which aims to quantify aseismic and seismic fault slip induced by fluid injections associated with hydraulic fracturing operations (Liu et al*.,* 2015).

2. The Numerical Code

2.1 Introduction to FLAC3D

The commercial software FLAC3D (Fast Lagrangian Analysis of Continua in 3 Dimensions) was selected to carry out the numerical simulation because it provides fully-coupled solutions to hydro-mechanical problems. Although primarily designed for geotechnical engineering purposes, FLAC3D can be used to model any type of problem in which a non-linear continuum analysis is required. To solve continuum mechanics problems, this explicit numerical code resorts to the finite-difference method which is a discretization technique used to obtain numerical solutions to differential equations. It involves approximating derivatives by algebraic expressions of finite differences (Morton and Mayers, 2005). In geomechanical problems, the governing differential equations relate the mechanical variable of stress to the kinematic variables of velocity and strain rate (ITASCA, 2011).

2.2 Validation of FLAC3D

In order to validate FLAC3D for induced seismicity applications, a benchmark problem was established. The results were compared to those obtained with FEPG (Finite Element Program Generator). This finite-element modeling code is known to yield accurate results for simple poroelastic diffusion problems. The benchmark problem consisted in prescribing a volumetric flow rate of 0.0001 m^3/s for a duration of 1 s and a time step of 0.001 s. The grid was a 1 x 1 x 1 m cube with uniform grid spacing of 0.05m. The results from the FLAC3D and FEPG simulations are shown in Figure 1.

It is evident from Figure 1 that the regular FLAC3D solution is numerically unstable compared to the FEPG solution. To resolve this discrepancy, mechanical sub-steps were introduced in the FLAC3D solving algorithm. The addition of mechanical sub-steps entails that for each fluid time increment, the program undergoes several mechanical steps to stabilize the system. This forced stabilization is necessary because the default FLAC3D algorithm assumes that the fluid-flow step is small enough that the system will re-equilibrate after only one mechanical step. This assumption fails in situations where fluid perturbations are the driving force. When mechanical sub-steps are used, the solutions obtained from FEPG and FLAC3D are essentially the same. FLAC3D was thus deemed adequate for the purpose of modeling fluid injection problems, as long as mechanical sub-steps are used.

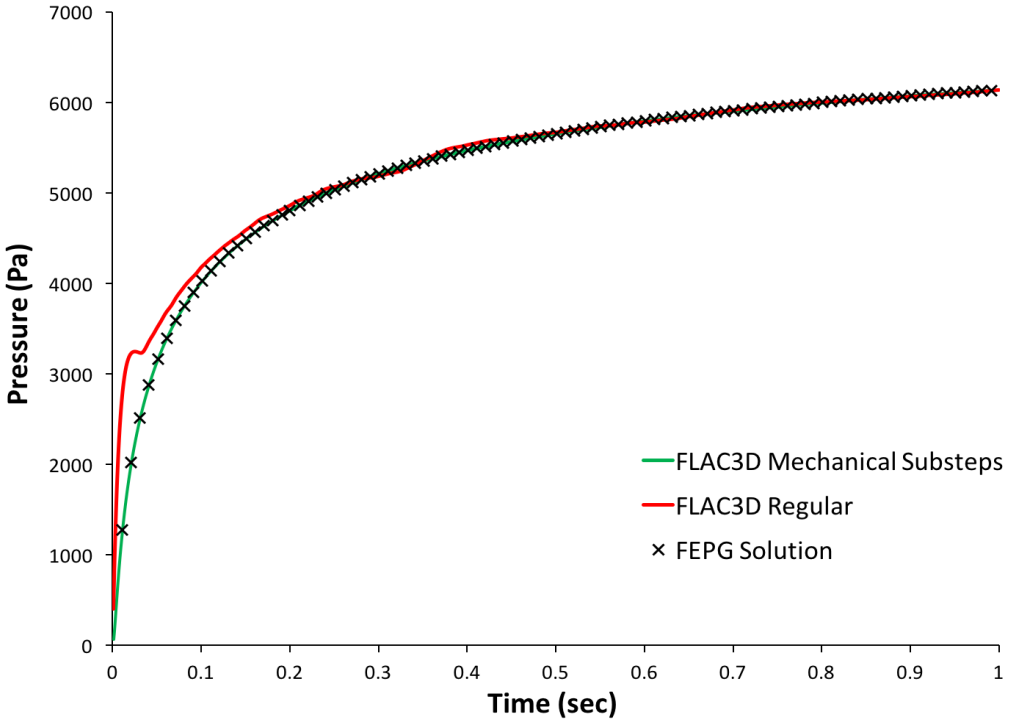

Figure 1: Comparison of modeling solutions for the validation problem.

3. Building the Model

Before the final model could be built, many tests had to be performed to determine the best way to represent the problem. More specifically, the type of fluid source, the fault modeling approach as well as the grid size all required further investigation.

3.1 The Fluid Source

FLAC3D offers three ways of simulating an inflow of fluid in a system. The first is to specify an increased pore pressure at a grid point. The extra pressure can be applied instantaneously or progressively through an optional input command. This approach is appealing because the pressures used in hydraulic fracturing operations are well documented in the industry. The second and third methods consist in implementing a constant flow rate at a grid point and at a zone, respectively.

The flow rate approach is advantageous because it allows the monitoring of both pore pressure and flow rate during the simulation. In the pressure approach, on the other hand, the flow rate cannot easily be back-calculated with FLAC3D. Since both the flow rate and the pore pressure are important in the characterization of an hydraulic fracturing injection, both should be readily available in the model. Furthermore, a grid point approach (as opposed to a volumetric approach) would be preferred because the injection well is small compared to the scale of the model considered. The injection well would thus be best represented by a point source with a constant flow rate (i.e., a constant flow rate at a gridpoint).

When the three approaches were tested in a simple model, we found that both the flow rate and increased pressure point sources yielded significantly different results depending on the grid size. Whereas it can be mathematically proven that a flow rate point source behaves as a singularity, the cause of the pressure point source divergence would require further investigation. Because results are trivial if they vary as a function of grid size, these two techniques had to be eliminated as viable options. The volumetric flow rate, on the other hand, gave similar results for all grid sizes tested. It was thus selected to simulate the fluid injection in the final model.

3.2 Fault Modeling Approaches

FLAC3D also offers different approaches to simulate fault planes. In the first approach, the fault is implemented via the "interface" command. An interface in FLAC3D is defined as a zero-thickness plane on which separation and sliding can occur. Although properties such as friction coefficient, dilation angle and cohesive strength can be specified, it is not possible to specify a permeability specific to the interface. Since a higher permeability at the fault zone is an important feature of the problem to be modeled (especially for an extensional fault at depth),, the interface approach is not appropriate in this case. Moreover, it is unrealistic to assume a plane with no thickness since real fault

planes do present a finite width. This width is filled with materials with properties diverging from the bulk crust.

An alternative approach is to represent the fault with finite thickness elements of weaker strength and higher permeability. However, it was unclear whether this artificial fault plane would be able to accommodate slip like an interface fault. Although modeling tests did confirm that weaker zones present higher differential movement than regular zones, the comparison between the interface and the finite thickness approaches is best explained by by a recent study on the modeling of fault reactivation induced by deep underground injection of CO_2 (Cappa and Rutqvist, 2011). This study found that by prescribing equivalent strength parameters for the two types of fault, both models could adequately simulate fault slip. The magnitudes of the slip were in agreement with one another as shown in Figure 2(d). Since the finite thickness element model is easier to implement and more representative of real faults, the authors decided to build their model with a finite thickness fault. The same approach was used for the present study.

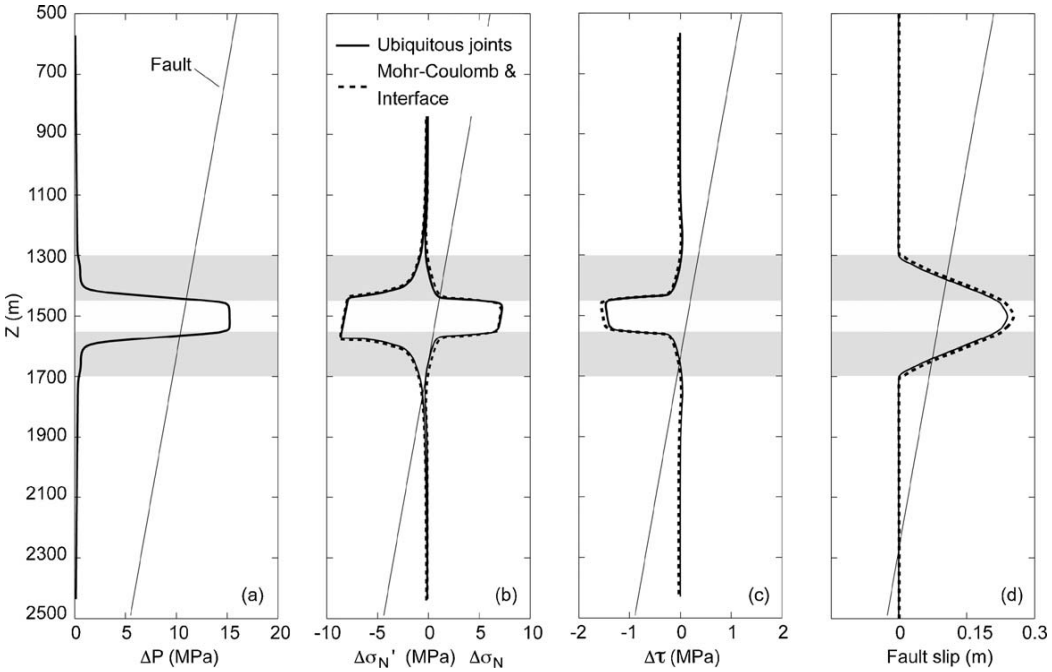

Figure 2: Pore pressure, normal stress, shear stress and slip along the fault depth for different fault modeling approaches. The interface and finite thickness fault models both coincide with the dash lines as the two profile overlap. The solid line represents an additional, more complex fault model that is not considered in this report. A 100m thick CO_2 reservoir is centered at depth 1500m, bounded by two caprock layers each of 150m of thickness (horizontal grey bars). (Cappa and Rutqvist, 2011).

3.3 Model and Grid Size Optimization

The model had to be large enough to (1) accommodate a fault spanning several kilometers and (2) prevent major boundary effects. For a fault of 6km in length and 5km in depth, the model was set at 16km in length, 18km in width and 7km in depth as shown in Figure 3. The validity of this model size is discussed in section 4.2. The first step in building the grid was to find the minimum grid size required to produce accurate results. With a simple test, it was shown that 500 m elements were sufficiently small to prevent grid effects and large enough to optimize the computation time. Figure 4 shows that the solution obtained with a grid size of 500m is within 4% agreement of that obtained with a 250m grid size. The 500 m solution took 18 minutes to compute while the 250 m solution took 2 hours and 10 minutes. It was concluded that the 4% gain in accuracy would not be worth the extra computation time.

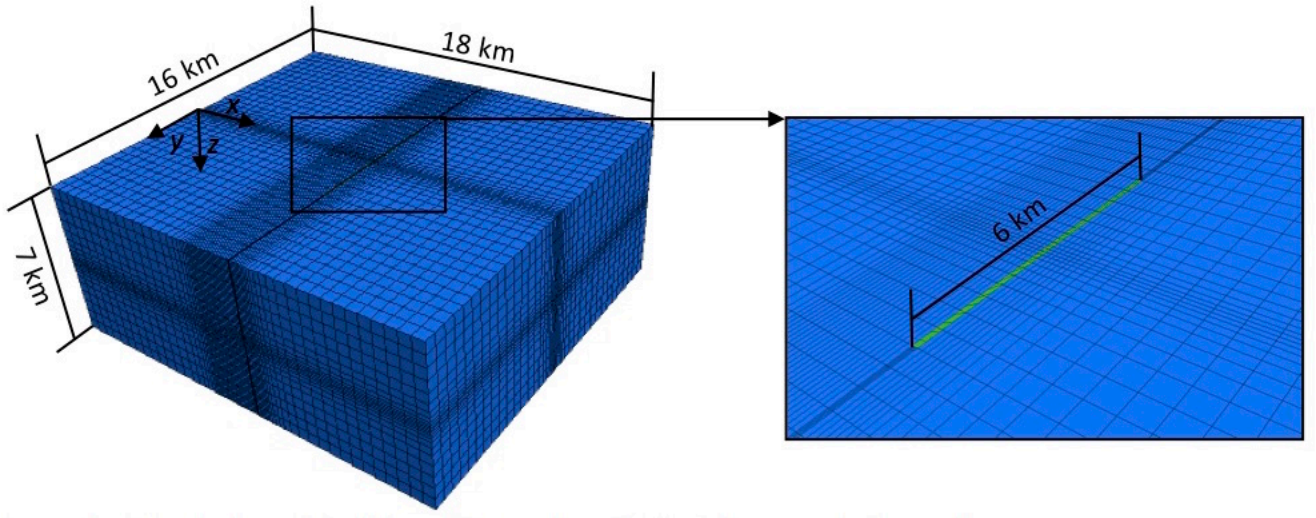

Figure 3: The final model grid and dimensions. The fault zone is shown in green.

This 500 m grid size is only applicable away from the area of interest. Because the size of the fluid source and fault thickness should be smaller than 500 m, the element size had to be reduced near these features. It was decided that a fault thickness of 100m would adequately simulate a fault zone. A fault zone includes the fault itself and the zone of increased permeability that surrounds it. The volumetric flow rate zone was similarly fixed at 100 x 100 x 100 m to make the grid as smooth and continuous as possible. Making a zone small enough to accommodate the actual size of a hydraulic fracturing well would result in an inconsistent grid and severely impede the computation process. Ultimately, it is

thought that the shape and size of the fluid source should have little influence on the resulting pore pressure and stress away from the source, as long as the actual pressure and flow rate are adequate.

Considering all of the above, a grid with progressively smaller elements near the fault zone and the volumetric fluid source was generated. The smallest elements in the model are in the fault zone and have a thickness of 25m, length of 100m and depth of 100m. The largest elements are 500x500x500 m cubes in the bulk crust away from the two main features. The final grid is illustrated in Figure 3.

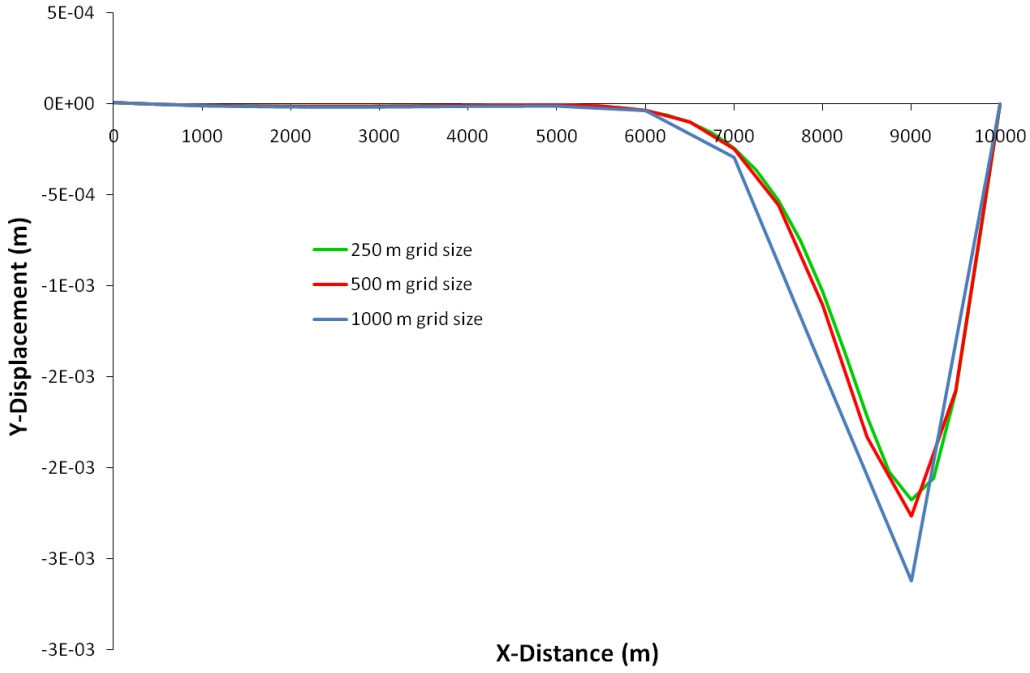

Figure 4: Comparison of grid sizes.

4. The Final Model

4.1 Model Parameters

The parameters for the model were first selected based on a typical elastic crust as presented in Table 1. The strength parameter (i.e., the shear modulus) was then decreased for the fault region, whereas the permeability and porosity were increased. The bulk crust was assumed to behave elastically while the fault region was considered to be a plastic-elastic medium as was the case with the model presented by Cappa and Rutqvist (2011). The Mohr-Coulomb failure criterion applies in the fault zone. Typical values of friction and dilation angles of 25º and 20º were used for the fault zone.

Table 1: Model parameters for fault and crust regions.

	Constitutive Model	*Shear Modulus*, μ (GPa)	*Poisson's Ratio*, ν	*Friction angle*, φ (°)	*Dilation angle*, ψ (°)	*Poro-sity*, ϕ (%)	*Permea-bility, k* (m^2)
Crust:	Elastic	30	0.25	-	-	2	5×10^{-16}
Fault:	Mohr-Coulomb	15	0.25	25	20	10	5×10^{-14}

4.2 Model Setup

All model boundaries are fixed and impermeable, except the ground surface which is free to move. When no fixity was specified at the four vertical boundaries, no significant change occurred for the variables sampled in the region of interest. Since the boundaries had little effect on the simulation results, the model dimensions with respect to the fault were deemed acceptable.

In terms of flow parameters, the objective was to simultaneously achieve a flow rate of 0.15 m^3/s and an increase in pore pressure of 60 MPa in 5 hours for an initial pore pressure of 0. These are the average values for the fluid injections associated with the Crooked Lake Sequences (Schultz et al., 2015). When a flow rate of 0.15 m^3/s was specified, however, the model only reached a pore pressure of 0.5 MPa. When the flow rate was increased by one order of magnitude to 1.5 m^3/s, the maximum pore pressure attained at the source was 63.6 MPa. It is suspected that the discrepancy between the numerical model and the field data might be due to errors in estimating material properties. For example, the permeability might have been underestimated and thus a higher flow rate was necessary to reach the desired pressure of 60 MPa in this period of time. This hypothesis would require further investigation.

The simulation was run with a flow rate of 1.5 m^3/s for 5 hours, after which the pumping was brought to a stop and the pressure was allowed to decay for about a week as illustrated in Figure 5. The fluid source is positioned at a depth of 3.5 km (the depth of the exploited shale formation near Fox Creek in Alberta (Schultz et al., 2015)) and 1 km away from the center of the fault. Any value could have been used for the distance between the source and the fault, but 1km was a good starting point.

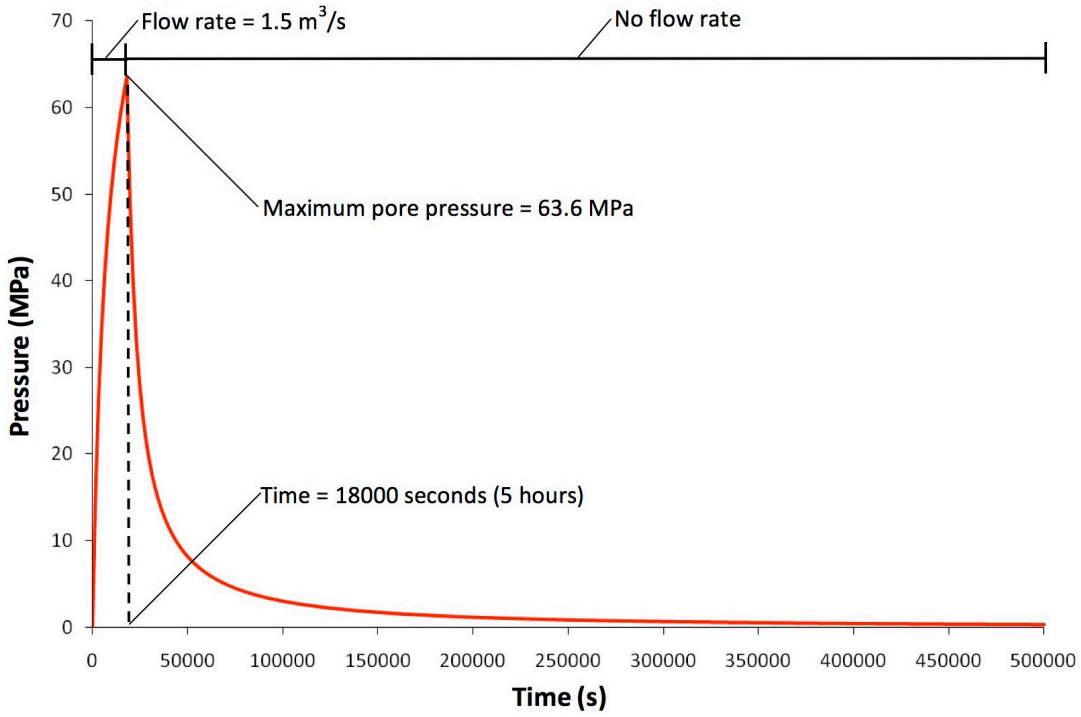

Figure 5: Pressure buildup and two-week decay at the injection source.

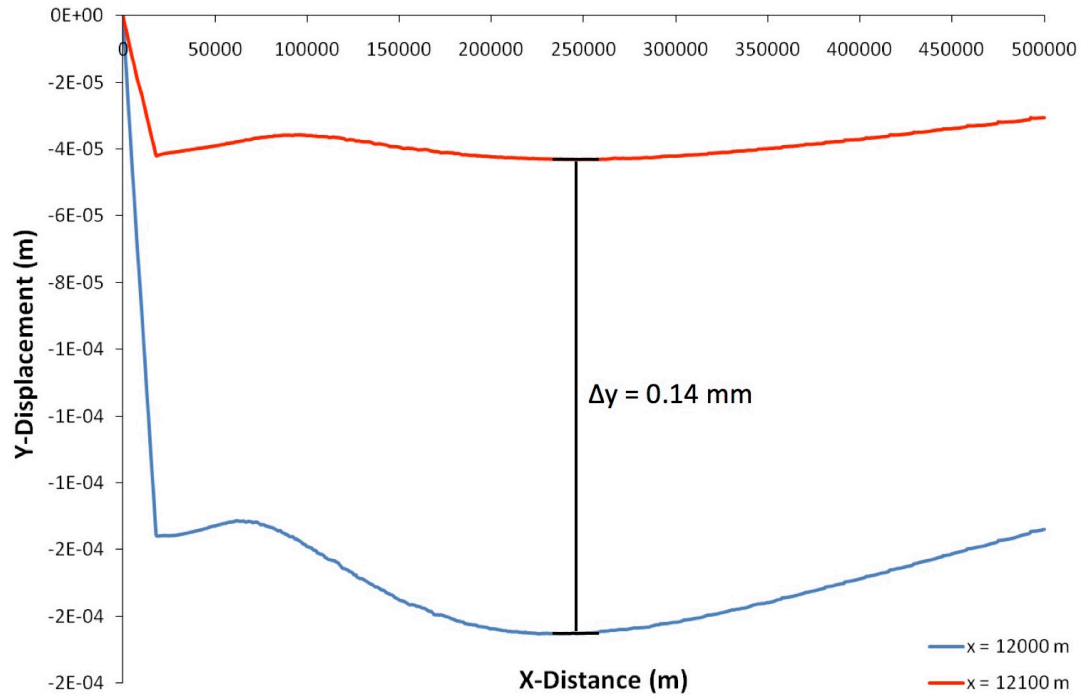

Figure 6: Evolution of y-displacement on either side of the fault 1km from the source in the y-direction.

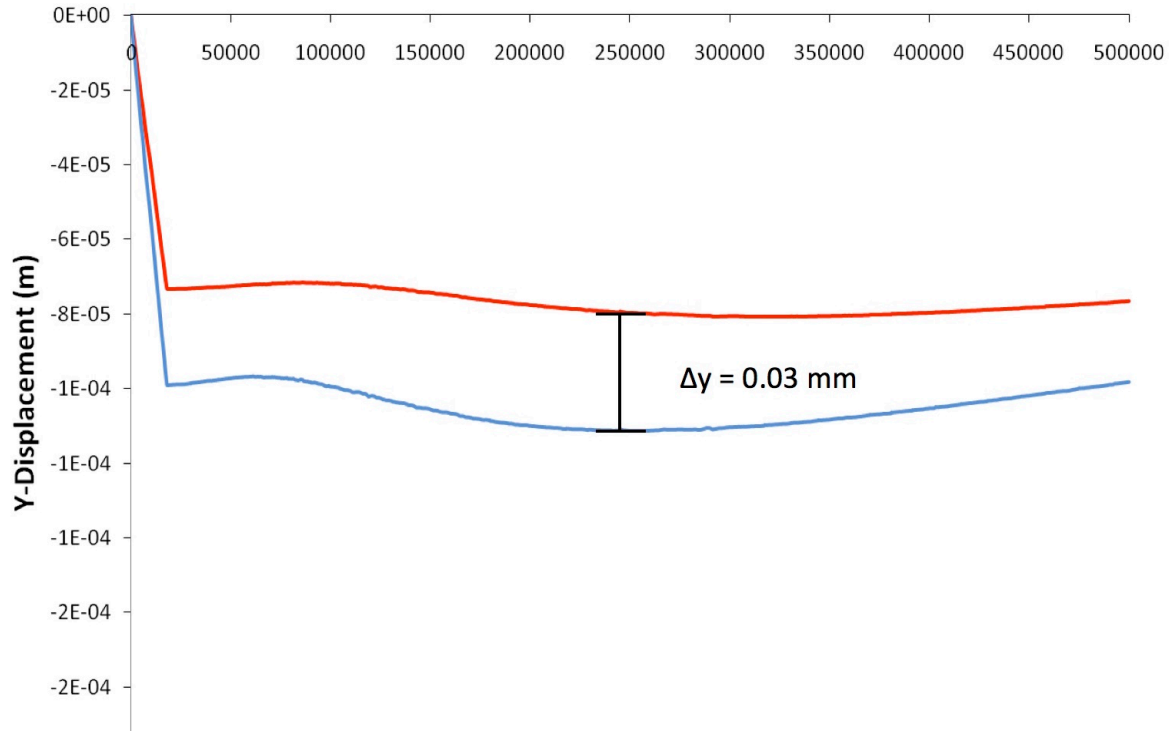

Figure 7: Evolution of y-displacement on either side of a point 1km from the source in the y-direction.

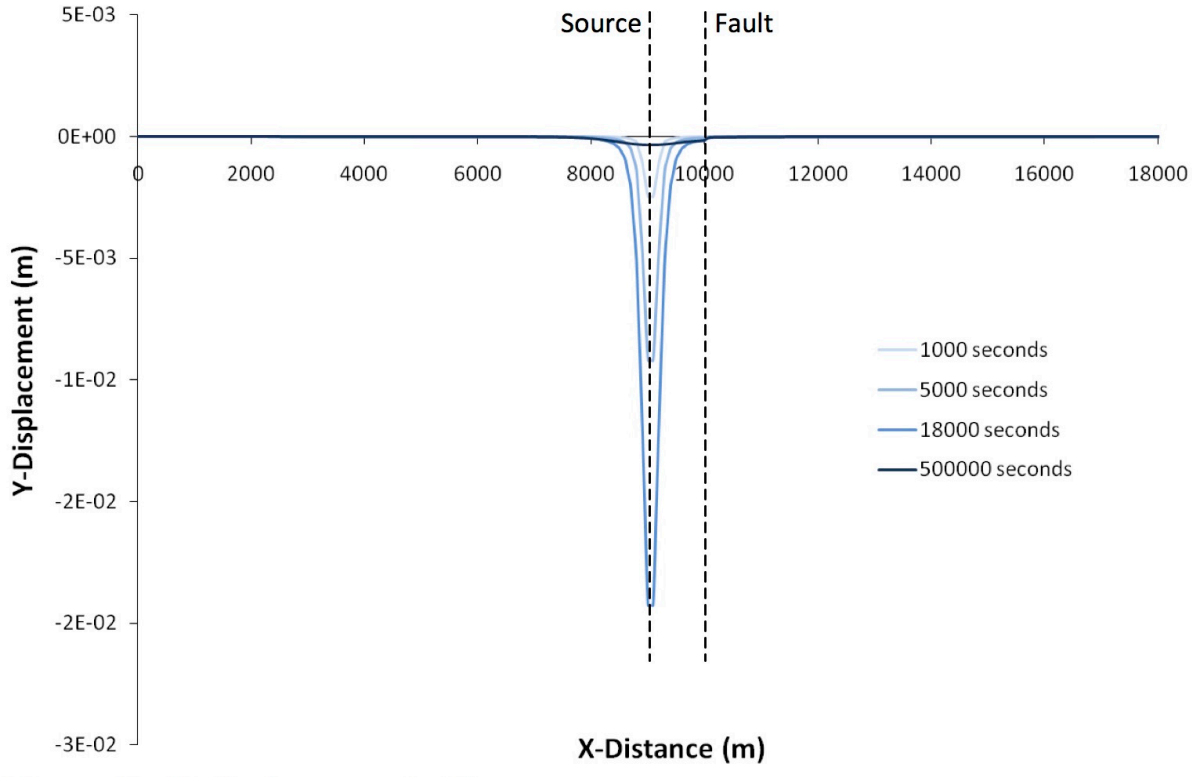

Figure 8: Y-displacement at the source.

4.3 Simulation Results

Y-displacement at the two faces of the fault zone was monitored throughout the simulation to determine the magnitude of the differential motion occurring at the faces of the fault. As can be observed in Figure 6, an maximum offset of 0.14 mm exists. The same measurement was taken on the opposite side of the source (where no fault is present) to establish how much of this offset is due to the spatial position of the two points. The offset in this case was 0.03 mm, as presented in Figure 7. Therefore, 0.11 mm of the total offset at the fault can be qualified as fault slip.

The y-displacement was also sampled across the entire model on planes perpendicular to the fault at different points in time. Figure 8 presents the results for a plane aligned at the source location. As would be expected from an elastic solid, the y-displacement increases with time when a flow rate is specified and slowly decreases back to zero upon removal of the perturbation.

When the plane is placed 1km away from the source, however, the smooth pattern is disrupted at the fault zone (Figure 9).

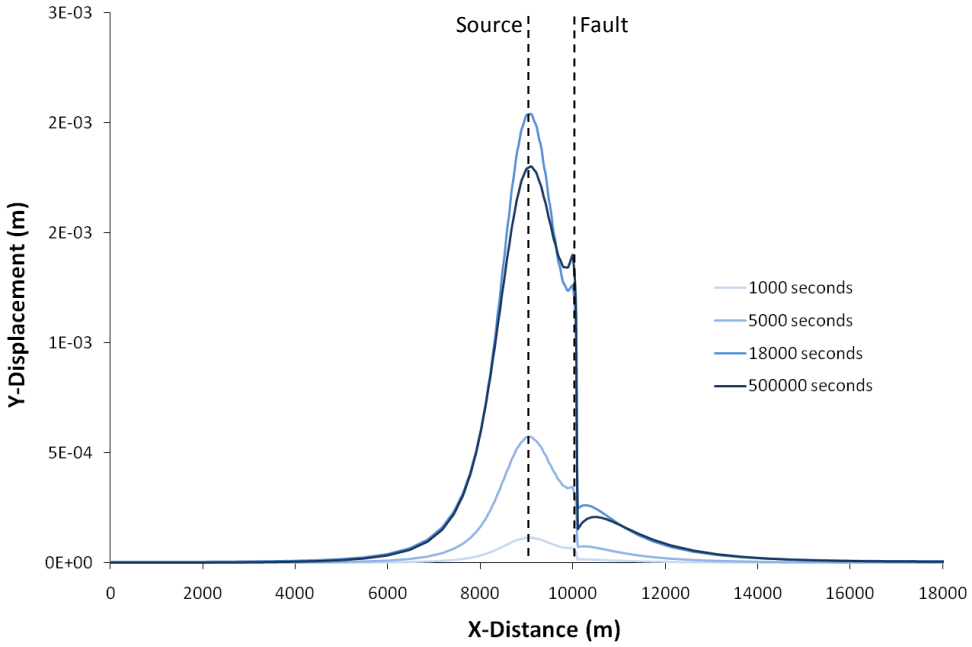

Figure 9: Y-displacement at 1 km from the source.

Similarly, when considering the xy-shear strain increment occurring on the same two planes, the curve is smooth for the plane at the source (Figure 10) and distorted for the plane at 1 km from the source (Figure 11).

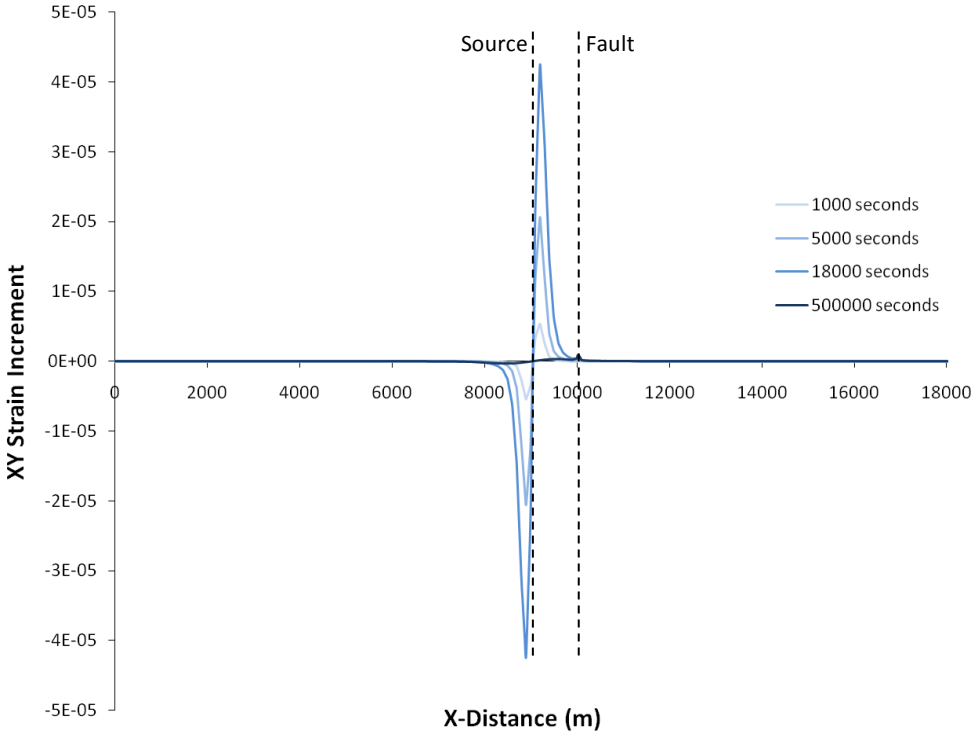

Figure 10: XY-Shear strain increment at the source.

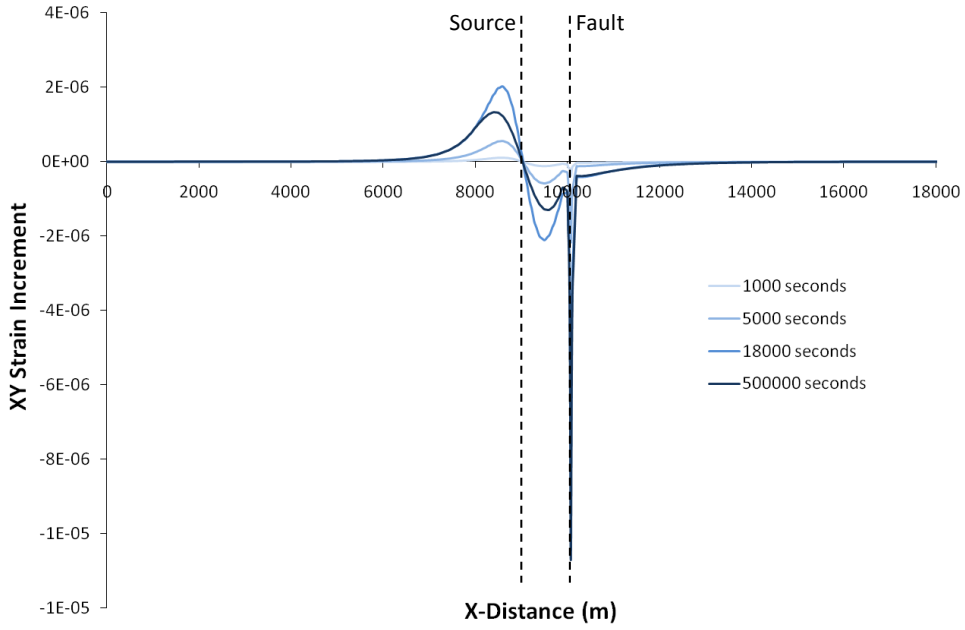

Figure 11: XY-Shear strain increment at 1km from the source.

The large spike in Figure 11 is most likely caused by plastic deformation at the fault zone as the curve stays in this shape even after 500000 seconds have elapsed (i.e., there is no elastic rebound at the

fault zone). This plastic deformation corroborates the hypothesis that slip occurs on the fault upon fluid injection.

Appendix B provides snapshots of pore pressure as well as normal and shear stresses at different points in time during the simulation.

4.4 Pore Pressure Front Propagation

Appendix B.7 and B.8 show isosurfaces of 0 and 1 kPa pore pressure fronts at different points in time. It can be seen from B.7 that, once established, the 0 pore pressure front stays relatively immobile. The 1 kPa pressure front, on the other hand, progresses significantly over time. By visual inspection, the average speed of the 1 kPa pressure front was estimated at 50 m/h (0.015 m/s) in the bulk crust and at 200 m/h (0.055 m/s) in the fault region. This increase in speed from the bulk crust to the fault region is expected given the higher permeability and weaker strength parameters of the fault.

5. Conclusions

In this numerical study, it was shown that a fault could be reactivated by a nearby fluid injection. The magnitude of the slip was 0.11 mm for this particular problem. This value should be considered with caution because numerous assumptions were made in arriving at this number. The fault slip observed in the field could be higher or lower than this particular value. Nonetheless, the aim of modeling fault slip induced by fluid injection in FLAC3D was achieved.

A major assumption made in the modeling process was that an elastic model could accurately represent the bulk crust whereas the fault zone could be represented by the plastic-elastic Mohr-Coulomb model. The strength parameters and material properties were also assumed without rigid proof from the field. The simulation should be repeated to determine how variations in constitutive models and model parameters affect the solution.

Further work on this topic will consist in informing the model with more precise hydraulic fracturing operational data and real geological data from the Fox Creek region. Rate-and-state friction will also be implemented in the model. Ultimately, the end goal of this research initiative would be to produce a map of fault structures in the region and see which ones are more prone to host seismic events when subjected to hydraulic fracturing injections.

6. Acknowledgements

We thank Dr. Denis Lavoie for constructive comments. This project was made possible thanks to the support of the Geological Survey of Canada (GSC), Natural Resources Canada (NRCan) who supplied the FLAC3D license for this project in the context of the Induced Seismicity Research Project of the Environmental Geoscience Program.

7. References

Atkinson, G. M., D. W. Eaton, H. Ghofrani, D. Walker, B. Cheadl1, R. Schultz, R. Shcherbakov, K. Tiampo, J. Gu, R. M. Harrington, Y. Liu, M. van der Baan, H. Kao. Hydraulic fracturing drives induced seismicity in the Western Canada Sedimentary Basin. *Seismological Research Letter*, in revision.

Biot, M. A., 1956. General solutions of the equations of elasticity and consolidation for a porous material. *Journal of Applied Mechanics*; volume 78, p. 91-96.

Cappa, F. and Rutqvist, J., 2011. Modeling of coupled deformation and permeability evolution during fault reactivation induced by deep underground injection of CO_2. *International Journal of Greenhouse Gas Control*; volume 5, p. 336-346.

Coulomb, C. A., 1776. Essai sur une application des règles des maximis et minimis à quelques problèmes de statique relatifs à l'architecture. *Mémoires de l'Académie Royale de Savoie*; volume 7, p. 343–387.

Detournay, E. and Cheng, A.H.-D., 1993. Fundamentals of poroelasticity. In *Comprehensive Rock Engineering: Principles, Practice and Projects*, Vol. 2. Pergamon Press, London, UK, p. 113-171.

Frohlich, C., 2012. Two-year survey comparing earthquake activity and injection-well locations in the Barnett Shale, Texas. *Proceedings of the National Academy of Sciences of the United States of America*; volume 34, p. 1-5.

ITASCA, 2011. Fast Lagrangian Analysis of Continua User's Guide, Version 7.0, ITASCA, Minnesota, USA.

Liu, Y., Harrington, R., Deng, K., and Larochelle, S., 2015. Modeling aseismic and seismic slip induced by fluid injection on pre-existing faults governed by rate-and-state friction, Abstract T52B-08 presented at 2015 Fall Meeting, AGU, San Francisco, Calif., 14-18 Dec.

McGarr, A., Simpson, D., and Seeber, L., 2002. Case histories of induced and triggered seismicity. In *International Handbook of Earthquake and Engineering Seismology,* Vol. 81A. Academic Press, San Francisco, USA, p. 647-661.

Morton, K. W., and Mayers, D.F., 2005. *Numerical solution of partial differential equations*. Cambridge University Press, New York, USA.

Raleigh, C. B., Healy, J.H., and Bredehoeft, J.D., 1976. An experiment in earthquake control at Rangely, Colorado. *Science*; volume 91, p. 1230-1237.

Rubinstein, J.L. and Mahani, A.B., 2015. Myths and facts on wastewater injection, hydraulic fracturing, enhanced oil recovery and induced seismicity. *Seismological Research Letters*; volume 86, p. 1060-1067.

Schultz, R., Stern, V., Novakovic, M., Atkinson, G., and Gu, Y.J., 2015. Hydraulic fracturing and the Crooked Lake Sequences: Insights gleaned from regional seismic networks. *Geophysical Research Letters*; volume 42, p. 2750-2758.

APPENDIX A
FLAC3D Code of the Final Model

; Grid generation

gen zone brick size 12 12 4 p0 2000 -8000 0 p1 8000 -8000 0 p2 2000 -2000 0 p3 2000 -8000 2000
gen zone brick ratio 1 1 0.75 size 12 12 6 p0 2000 -8000 2000 p1 8000 -8000 2000 p2 2000 -2000 2000 p3 2000 -8000 3400
gen zone brick size 12 12 2 p0 2000 -8000 3400 p1 8000 -8000 3400 p2 2000 -2000 3400 p3 2000 -8000 3600
gen zone brick ratio 1 1 1.33333 size 12 12 6 p0 2000 -8000 3600 p1 8000 -8000 3600 p2 2000 -2000 3600 p3 2000 -8000 5000
gen zone brick size 12 12 4 p0 2000 -8000 5000 p1 8000 -8000 5000 p2 2000 -2000 5000 p3 2000 -8000 7000

gen zone brick ratio 1 .8 1 size 12 8 4 p0 2000 -2000 0 p1 8000 -2000 0 p2 2000 0 0 p3 2000 -2000 2000
gen zone brick ratio 1 .8 0.75 size 12 8 6 p0 2000 -2000 2000 p1 8000 -2000 2000 p2 2000 0 2000 p3 2000 -2000 3400
gen zone brick ratio 1 .8 1 size 12 8 2 p0 2000 -2000 3400 p1 8000 -2000 3400 p2 2000 0 3400 p3 2000 -2000 3600
gen zone brick ratio 1 .8 1.33333 size 12 8 6 p0 2000 -2000 3600 p1 8000 -2000 3600 p2 2000 0 3600 p3 2000 -2000 5000
gen zone brick ratio 1 .8 1 size 12 8 4 p0 2000 -2000 5000 p1 8000 -2000 5000 p2 2000 0 5000 p3 2000 -2000 7000

gen zone brick size 12 1 4 p0 2000 0 0 p1 8000 0 0 p2 2000 100 0 p3 2000 0 2000
gen zone brick ratio 1 1 0.75 size 12 1 6 p0 2000 0 2000 p1 8000 0 2000 p2 2000 100 2000 p3 2000 0 3400
gen zone brick size 12 1 2 p0 2000 0 3400 p1 8000 0 3400 p2 2000 100 3400 p3 2000 0 3600
gen zone brick ratio 1 1 1.33333 size 12 1 6 p0 2000 0 3600 p1 8000 0 3600 p2 2000 100 3600 p3 2000 0 5000
gen zone brick size 12 1 4 p0 2000 0 5000 p1 8000 0 5000 p2 2000 100 5000 p3 2000 0 7000

gen zone brick ratio 0.8 1 1 size 8 12 4 p0 8000 -8000 0 p1 10000 -8000 0 p2 8000 -2000 0 p3 8000 -8000 2000
gen zone brick ratio 0.8 1 0.75 size 8 12 6 p0 8000 -8000 2000 p1 10000 -8000 2000 p2 8000 -2000 2000 p3 8000 -8000 3400
gen zone brick ratio 0.8 1 1 size 8 12 2 p0 8000 -8000 3400 p1 10000 -8000 3400 p2 8000 -2000 3400 p3 8000 -8000 3600
gen zone brick ratio 0.8 1 1.33333 size 8 12 6 p0 8000 -8000 3600 p1 10000 -8000 3600 p2 8000 -2000 3600 p3 8000 -8000 5000
gen zone brick ratio 0.8 1 1 size 8 12 4 p0 8000 -8000 5000 p1 10000 -8000 5000 p2 8000 -2000 5000 p3 8000 -8000 7000

gen zone brick size 20 12 4 p0 10000 -8000 0 p1 12000 -8000 0 p2 10000 -2000 0 p3 10000 -8000 2000
gen zone brick ratio 1 1 0.75 size 20 12 6 p0 10000 -8000 2000 p1 12000 -8000 2000 p2 10000 -2000 2000 p3 10000 -8000 3400
gen zone brick size 20 12 2 p0 10000 -8000 3400 p1 12000 -8000 3400 p2 10000 -2000 3400 p3 10000 -8000 3600
gen zone brick ratio 1 1 1.33333 size 20 12 6 p0 10000 -8000 3600 p1 12000 -8000 3600 p2 10000 -2000 3600 p3 10000 -8000 5000
gen zone brick size 20 12 4 p0 10000 -8000 5000 p1 12000 -8000 5000 p2 10000 -2000 5000 p3 10000 -8000 7000

gen zone brick ratio 0.8 0.8 1 size 8 8 4 p0 8000 -2000 0 p1 10000 -2000 0 p2 8000 0 0 p3 8000 -2000 2000
gen zone brick ratio 0.8 0.8 0.75 size 8 8 6 p0 8000 -2000 2000 p1 10000 -2000 2000 p2 8000 0 2000 p3 8000 -2000 3400
gen zone brick ratio 0.8 0.8 1 size 8 8 2 p0 8000 -2000 3400 p1 10000 -2000 3400 p2 8000 0 3400 p3 8000 -2000 3600
gen zone brick ratio 0.8 0.8 1.33333 size 8 8 6 p0 8000 -2000 3600 p1 10000 -2000 3600 p2 8000 0 3600 p3 8000 -2000 5000
gen zone brick ratio 0.8 0.8 1 size 8 8 4 p0 8000 -2000 5000 p1 10000 -2000 5000 p2 8000 0 5000 p3 8000 -2000 7000

gen zone brick ratio 0.8 1 1 size 8 1 4 p0 8000 0 0 p1 10000 0 0 p2 8000 100 0 p3 8000 0 2000
gen zone brick ratio 0.8 1 0.75 size 8 1 6 p0 8000 0 2000 p1 10000 0 2000 p2 8000 100 2000 p3 8000 0 3400
gen zone brick ratio 0.8 1 1 size 8 1 2 p0 8000 0 3400 p1 10000 0 3400 p2 8000 100 3400 p3 8000 0 3600
gen zone brick ratio 0.8 1 1.33333 size 8 1 6 p0 8000 0 3600 p1 10000 0 3600 p2 8000 100 3600 p3 8000 0 5000
gen zone brick ratio 0.8 1 1 size 8 1 4 p0 8000 0 5000 p1 10000 0 5000 p2 8000 100 5000 p3 8000 0 7000

gen zone brick ratio 1 0.8 1 size 20 8 4 p0 10000 -2000 0 p1 12000 -2000 0 p2 10000 0 0 p3 10000 -2000 2000
gen zone brick ratio 1 0.8 0.75 size 20 8 6 p0 10000 -2000 2000 p1 12000 -2000 2000 p2 10000 0 2000 p3 10000 -2000 3400
gen zone brick ratio 1 0.8 1 size 20 8 2 p0 10000 -2000 3400 p1 12000 -2000 3400 p2 10000 0 3400 p3 10000 -2000 3600
gen zone brick ratio 1 0.8 1.33333 size 20 8 6 p0 10000 -2000 3600 p1 12000 -2000 3600 p2 10000 0 3600 p3 10000 -2000 5000
gen zone brick ratio 1 0.8 1 size 20 8 4 p0 10000 -2000 5000 p1 12000 -2000 5000 p2 10000 0 5000 p3 10000 -2000 7000

gen zone brick ratio 1 1 1 size 20 1 4 p0 10000 0 0 p1 12000 0 0 p2 10000 100 0 p3 10000 0 2000
gen zone brick ratio 1 1 0.75 size 20 1 6 p0 10000 0 2000 p1 12000 0 2000 p2 10000 100 2000 p3 10000 0 3400
gen zone brick ratio 1 1 1 size 20 1 2 p0 10000 0 3400 p1 12000 0 3400 p2 10000 100 3400 p3 10000 0 3600
gen zone brick ratio 1 1 1.33333 size 20 1 6 p0 10000 0 3600 p1 12000 0 3600 p2 10000 100 3600 p3 10000 0 5000
gen zone brick ratio 1 1 1 size 20 1 4 p0 10000 0 5000 p1 12000 0 5000 p2 10000 100 5000 p3 10000 0 7000

gen zone brick ratio 1 1 1 size 4 10 4 p0 12000 -8000 0 p1 12100 -8000 0 p2 12000 -3000 0 p3 12000 -8000 2000
gen zone brick ratio 1 1 0.75 size 4 10 6 p0 12000 -8000 2000 p1 12100 -8000 2000 p2 12000 -3000 2000 p3 12000 -8000 3400
gen zone brick ratio 1 1 1 size 4 10 2 p0 12000 -8000 3400 p1 12100 -8000 3400 p2 12000 -3000 3400 p3 12000 -8000 3600
gen zone brick ratio 1 1 1.33333 size 4 10 6 p0 12000 -8000 3600 p1 12100 -8000 3600 p2 12000 -3000 3600 p3 12000 -8000 5000
gen zone brick ratio 1 1 1 size 4 10 4 p0 12000 -8000 5000 p1 12100 -8000 5000 p2 12000 -3000 5000 p3 12000 -8000 7000

```
group crust

gen zone brick ratio 1 1 1 size 4 2 4 p0 12000 -3000 0 p1 12100 -3000 0 p2 12000 -2000 0 p3 12000 -3000 2000 group fault
gen zone brick ratio 1 1 0.75 size 4 2 6 p0 12000 -3000 2000 p1 12100 -3000 2000 p2 12000 -2000 2000 p3 12000 -3000 3400 group
fault
gen zone brick ratio 1 1 1 size 4 2 2 p0 12000 -3000 3400 p1 12100 -3000 3400 p2 12000 -2000 3400 p3 12000 -3000 3600 group fault
gen zone brick ratio 1 1 1.33333 size 4 2 6 p0 12000 -3000 3600 p1 12100 -3000 3600 p2 12000 -2000 3600 p3 12000 -3000 5000 group
fault
gen zone brick ratio 1 1 1 size 4 2 4 p0 12000 -3000 5000 p1 12100 -3000 5000 p2 12000 -2000 5000 p3 12000 -3000 7000 group crust

gen zone brick ratio 1 0.8 1 size 4 8 4 p0 12000 -2000 0 p1 12100 -2000 0 p2 12000 0 0 p3 12000 -2000 2000 group fault
gen zone brick ratio 1 0.8 0.75 size 4 8 6 p0 12000 -2000 2000 p1 12100 -2000 2000 p2 12000 0 2000 p3 12000 -2000 3400 group fault
gen zone brick ratio 1 0.8 1 size 4 8 2 p0 12000 -2000 3400 p1 12100 -2000 3400 p2 12000 0 3400 p3 12000 -2000 3600 group fault
gen zone brick ratio 1 0.8 1.33333 size 4 8 6 p0 12000 -2000 3600 p1 12100 -2000 3600 p2 12000 0 3600 p3 12000 -2000 5000 group
fault
gen zone brick ratio 1 0.8 1 size 4 8 4 p0 12000 -2000 5000 p1 12100 -2000 5000 p2 12000 0 5000 p3 12000 -2000 7000 group crust

gen zone brick ratio 1 1 1 size 4 1 4 p0 12000 0 0 p1 12100 0 0 p2 12000 100 0 p3 12000 0 2000 group fault
gen zone brick ratio 1 1 0.75 size 4 1 6 p0 12000 0 2000 p1 12100 0 2000 p2 12000 100 2000 p3 12000 0 3400 group fault
gen zone brick ratio 1 1 1 size 4 1 2 p0 12000 0 3400 p1 12100 0 3400 p2 12000 100 3400 p3 12000 0 3600 group fault
gen zone brick ratio 1 1 1.33333 size 4 1 6 p0 12000 0 3600 p1 12100 0 3600 p2 12000 100 3600 p3 12000 0 5000 group fault
gen zone brick ratio 1 1 1 size 4 1 4 p0 12000 0 5000 p1 12100 0 5000 p2 12000 100 5000 p3 12000 0 7000 group crust

gen zone reflect dip 90 dd 0 origin 0 50 0 range y -8000 0
gen zone reflect dip 90 dd 90 origin 11300 0 0 range x 2500 10500

; Prescribe constitutive models

model mech mohr range group fault
prop young 5e9 poisson 0.25 range group fault
prop fric 25 dilation 20 tens 2.1445e7 range group fault

model mech elastic range group crust
prop young 10e9 poisson 0.25 range group crust

; Specify boundary conditions

fix x range x 2000
fix x range x 20100
fix y range y -8000
fix y range y 8100
fix z range z 7000

; Specify flow properties

config fluid
model fluid fl_iso
ini fmod 2e9
ini sat 1
prop poros 0.02 perm 1e-12 range group crust
prop poros 0.10 perm 1e-10 range group fault

apply vwell 1.5e-6 range x 11000 11100 y 0 100 z 3400 3500

set fluid dt 100
set mech force 0 ratio 1e-3
set mech subs 10000 auto
set fluid subs 100
```

APPENDIX B

Pore Pressure and Stress Snapshots from the Simulation

1) Pore pressure across the fault

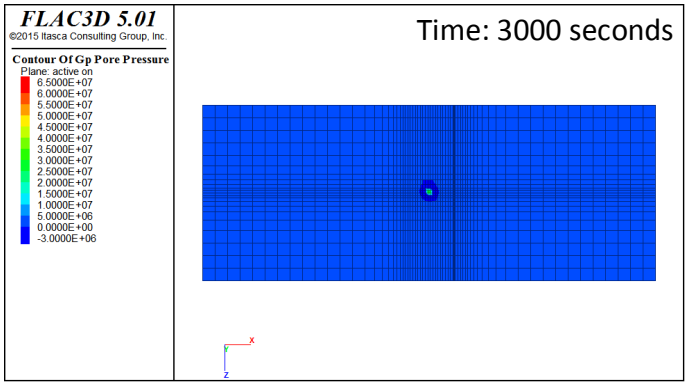

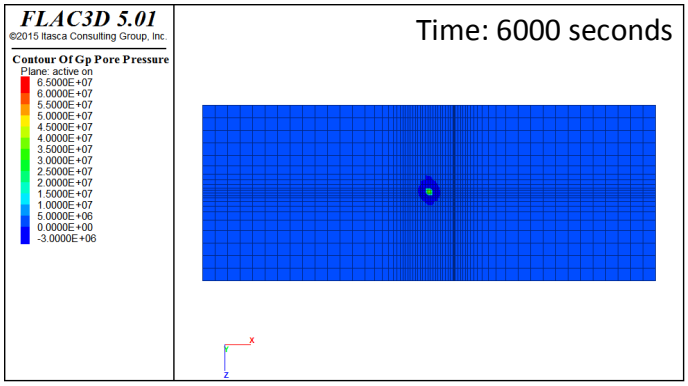

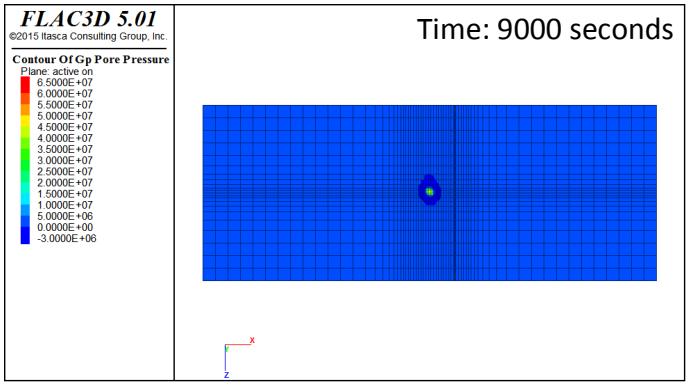

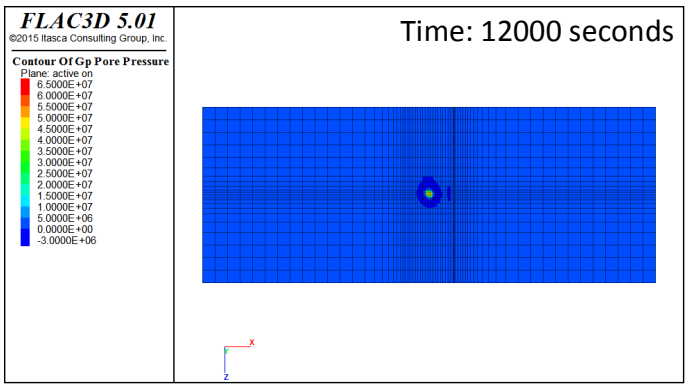

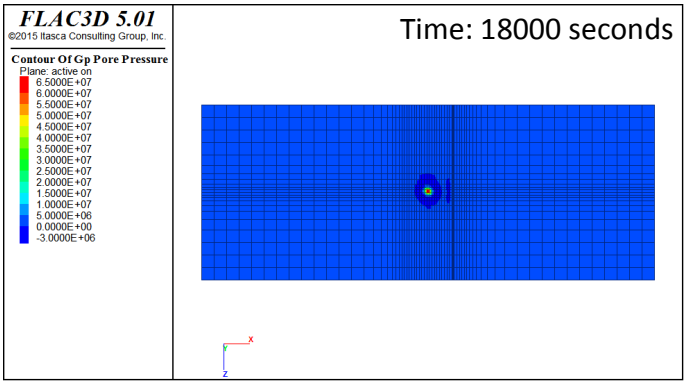

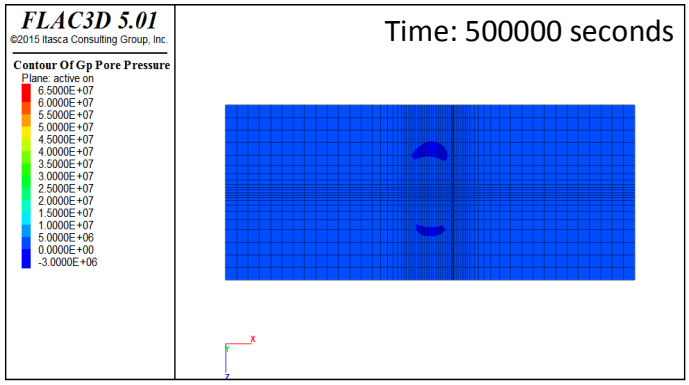

2) Pore pressure along the fault

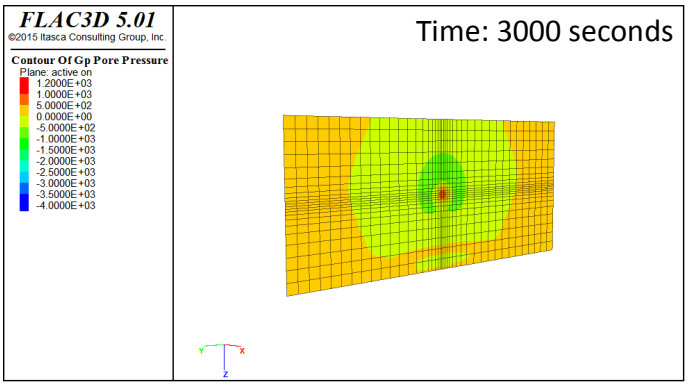

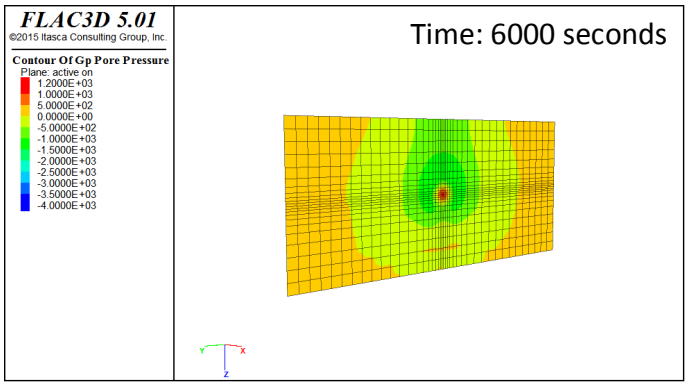

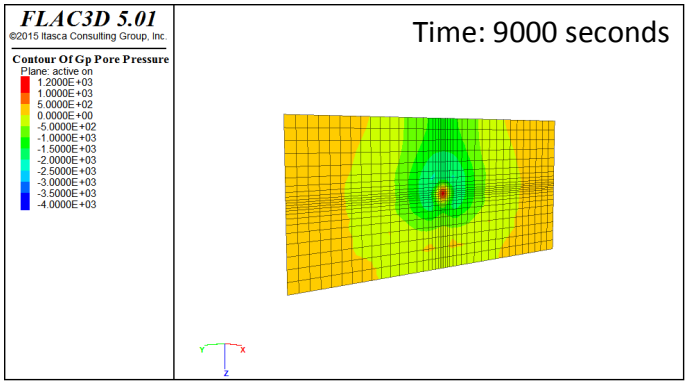

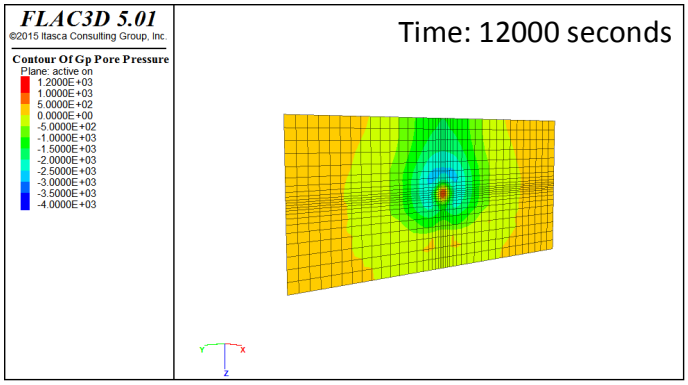

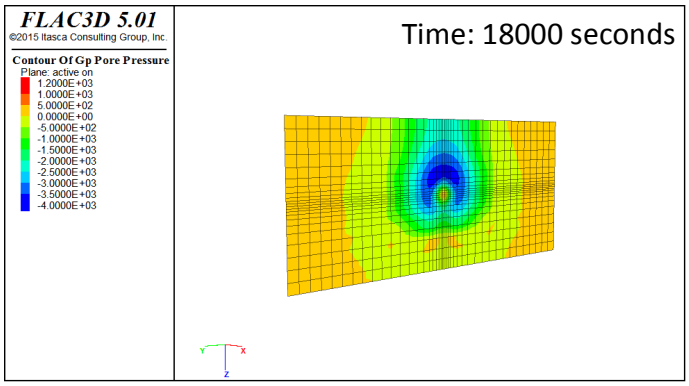

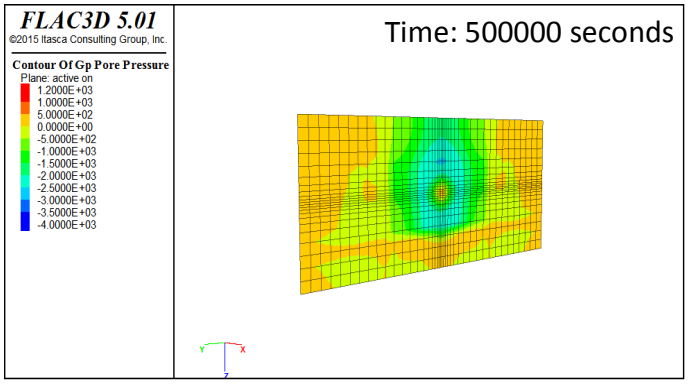

3) Shear stress across the fault

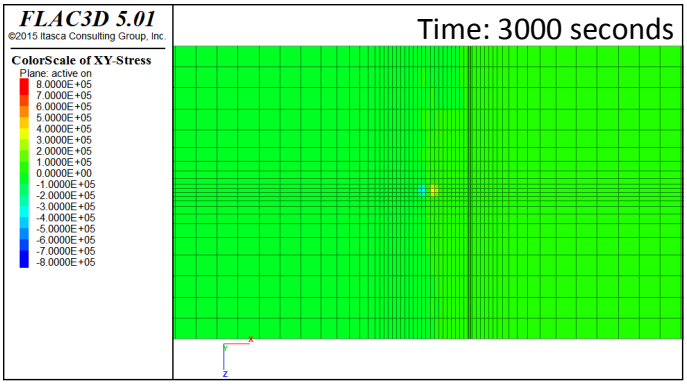

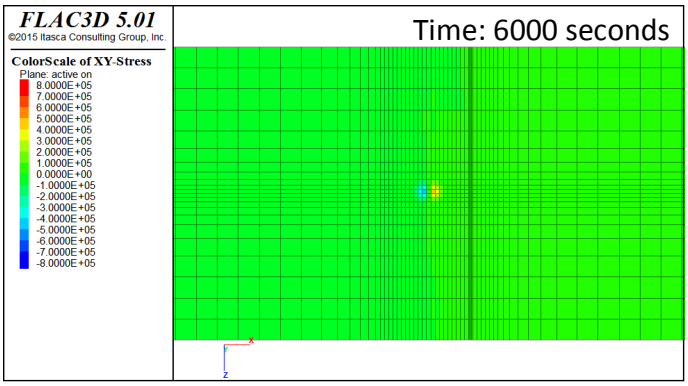

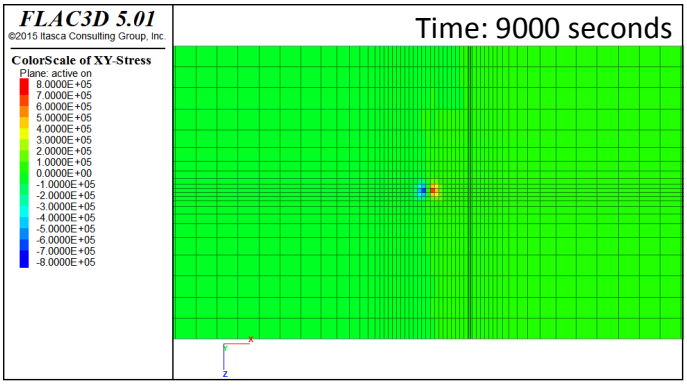

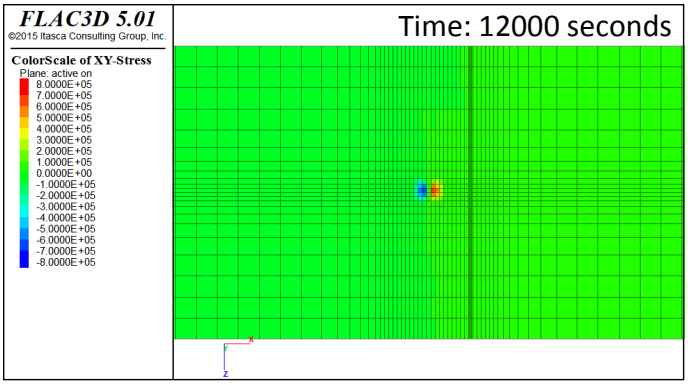

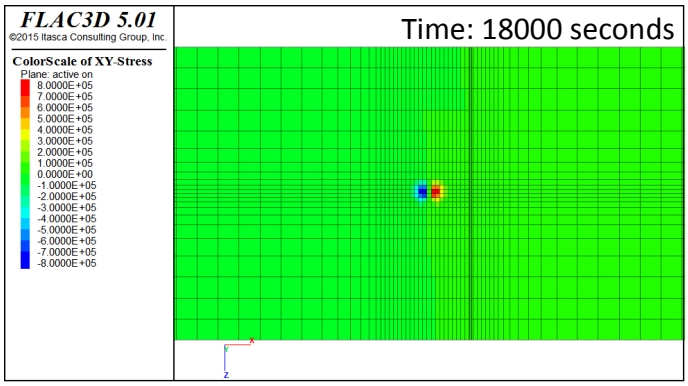

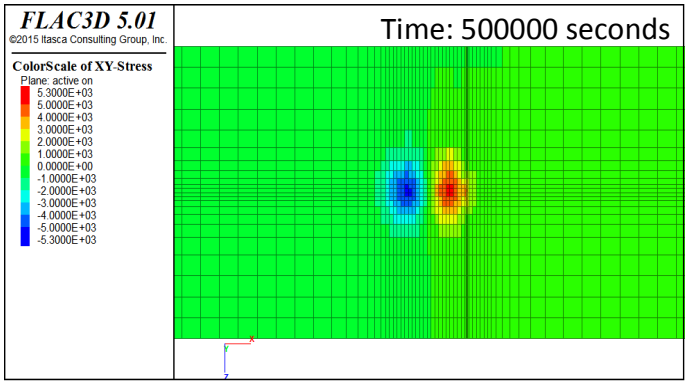

***Note:** The color scale was changed here to show the distribution of shear stresses on the opposite side of the fault.

4) Shear stress along the fault

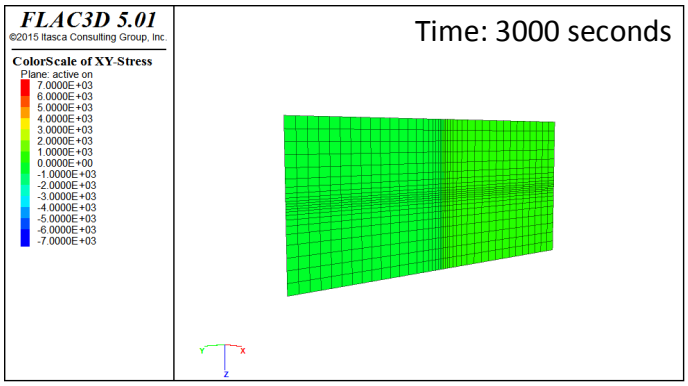

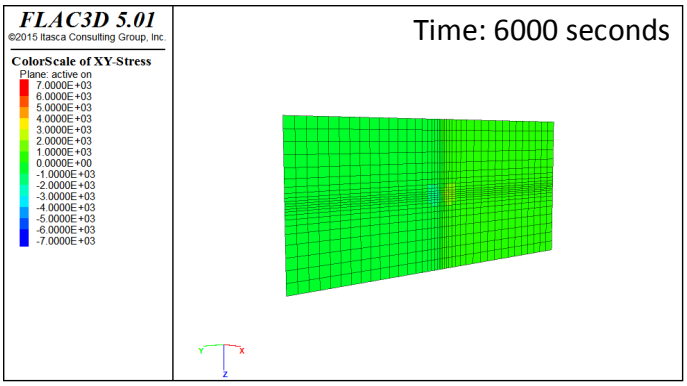

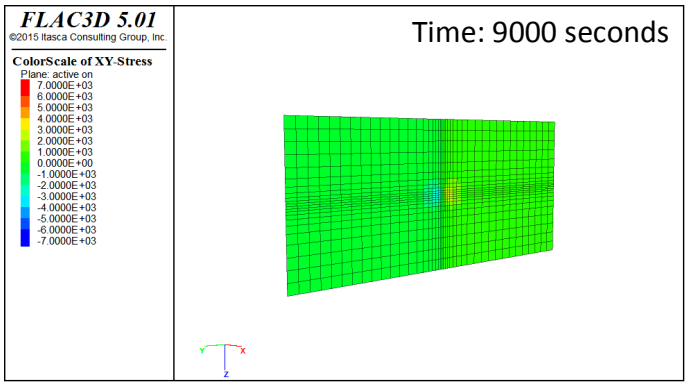

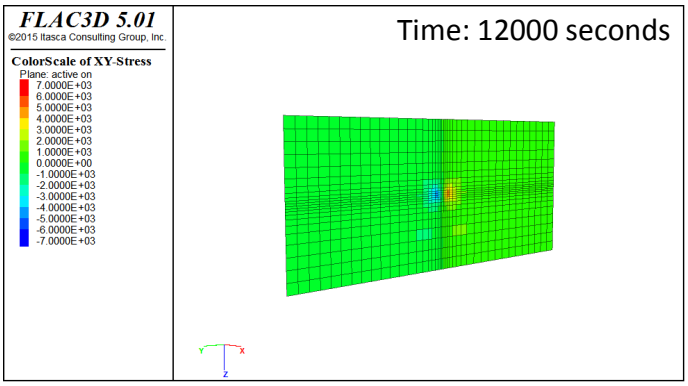

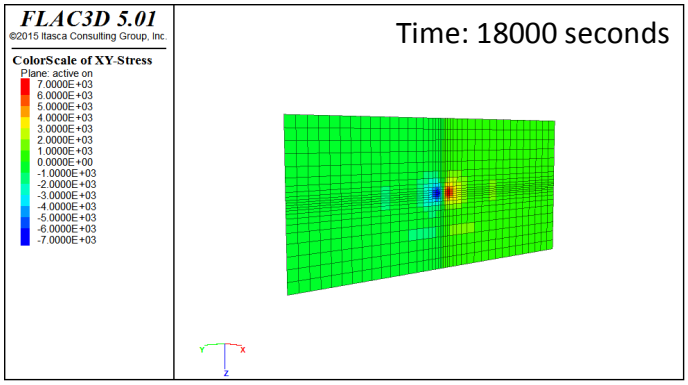

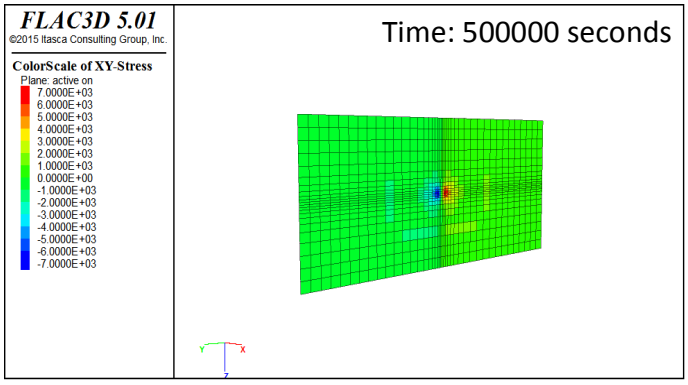

5) Normal stress across the fault

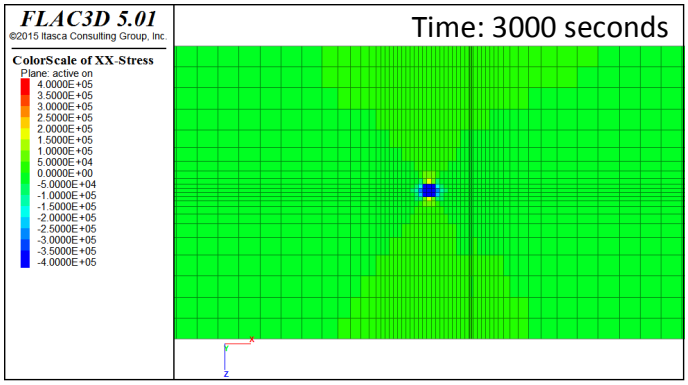

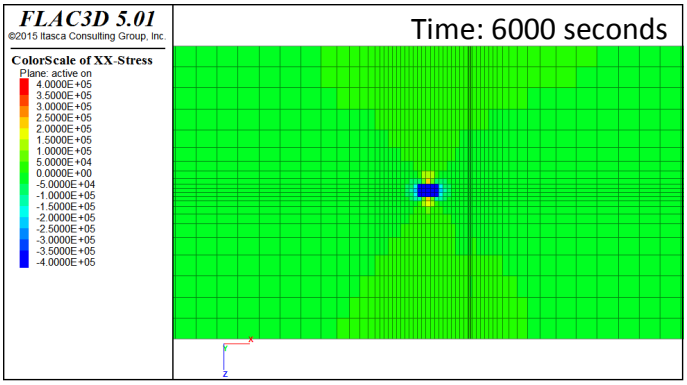

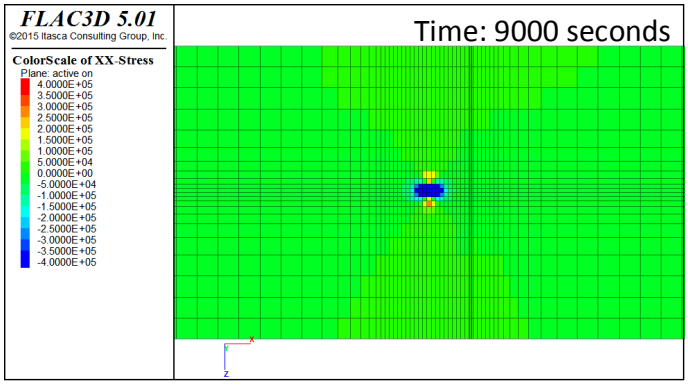

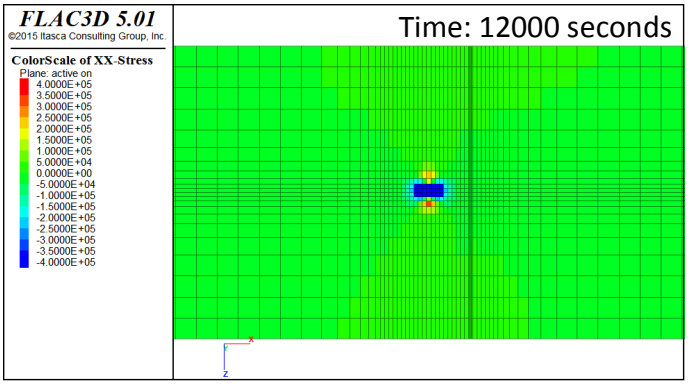

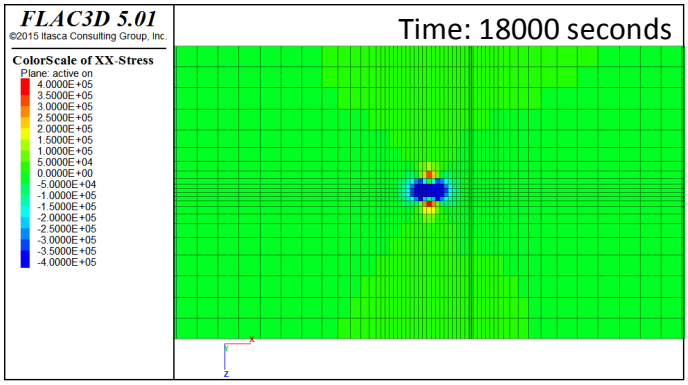

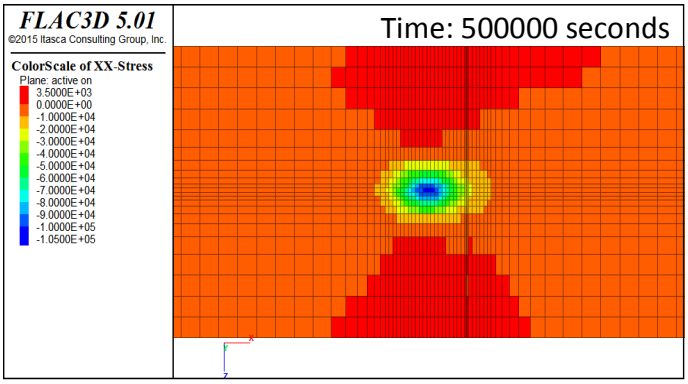

***Note:** The color scale was changed here to show the distribution of normal stresses on the opposite side of the fault.

6) Normal stress along the fault

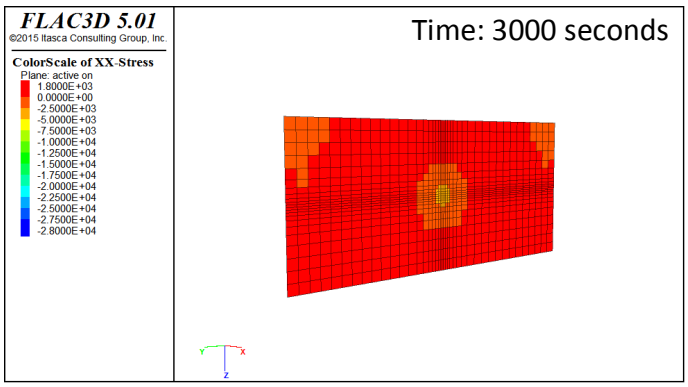

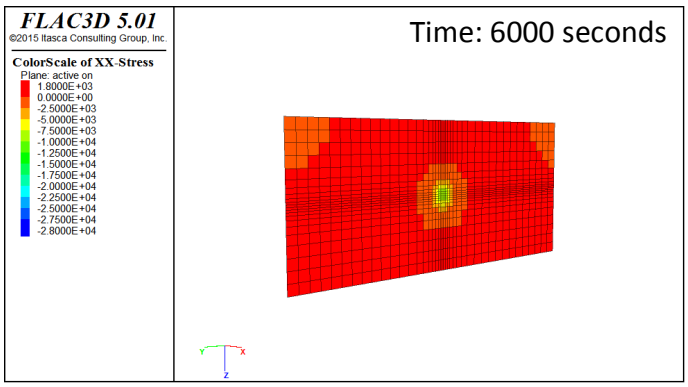

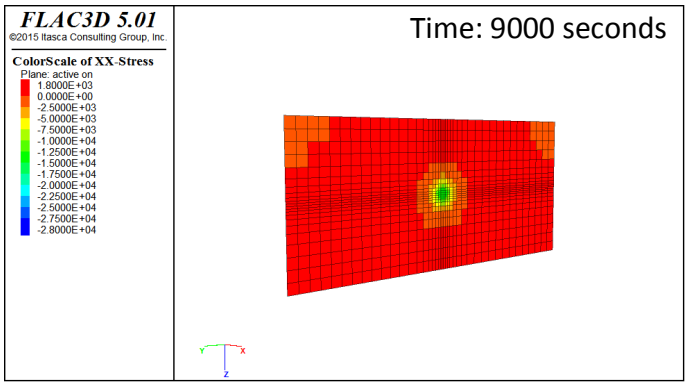

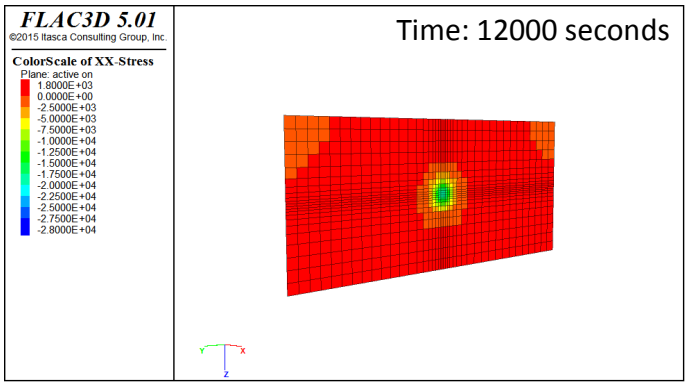

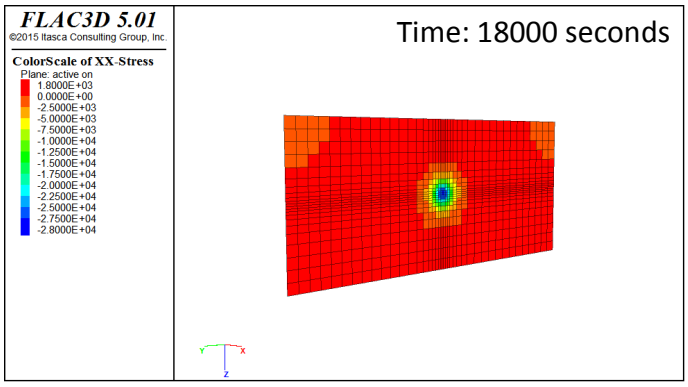

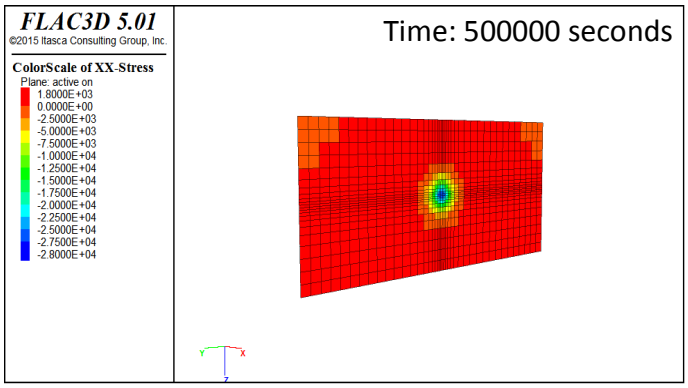

7) 0 kPa Pressure Front

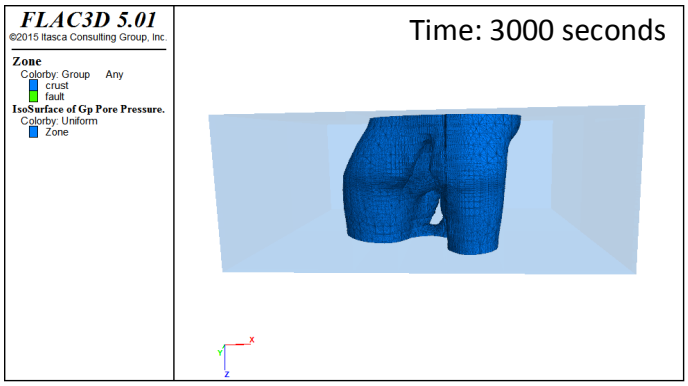

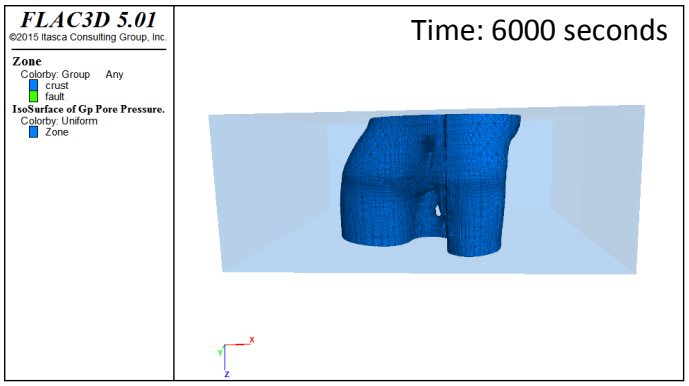

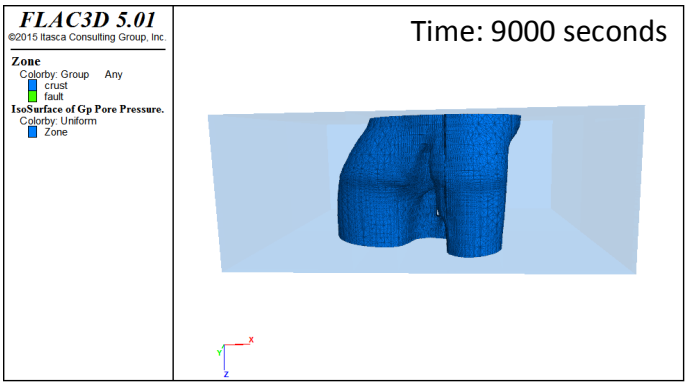

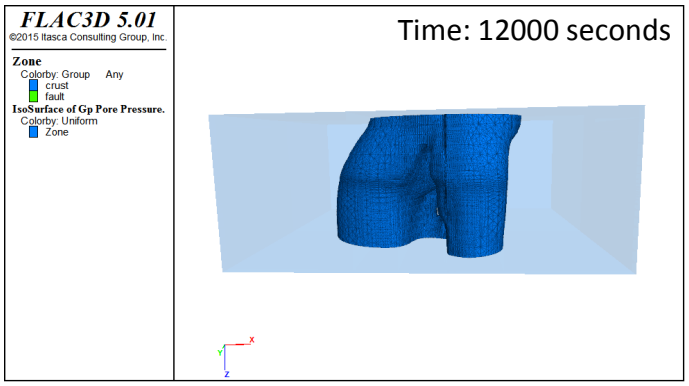

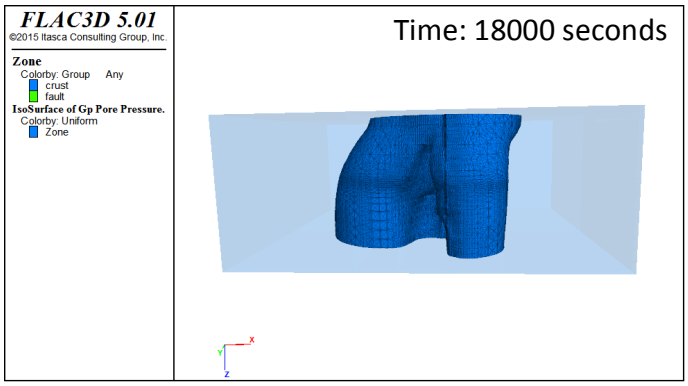

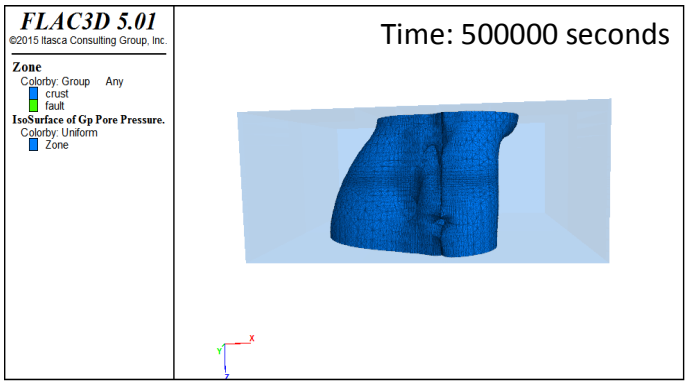

8) 1 kPa Pressure Front